Materials Research. 2024; 27(suppl. 2):e20240232
DOI: https://doi.org/10.1590/1980-5373-MR-2024-0232

Analysis of thin Film Deposition and Defects Influence on Quinoline Derivative-Titanium Dioxide Heterostructure for Potential p-n Junction in Optoelectronic Devices

***Natália C. Oliveira*[a,b], *Lucas P. Fonseca*[a], *Luis V.A. Scalvi*[a*]**

[a]*Universidade Estadual Paulista, Laboratório de Experimentos Electro-Ópticos em Materiais, Departamento de Física e Meteorologia, Faculdade de Ciências, Programa de Pós-Graduação em Ciência e Tecnologia de Materiais, Bauru, SP, Brasil.*
[b]*Universidade Estadual Paulista, Departamento de Química, Faculdade de Ciências, Bauru, SP, Brasil.*

Received: May 20, 2024; Revised: July 19, 2024; Accepted: August 15, 2024

Titanium dioxide (TiO_2) is an n-type oxide semiconductor, where the electron donors are usually associated with oxygen vacancies and interstitial titanium ions, whereas quinoline derivatives (QD) are usually p-type semiconductors with light emission in the blue range. We report a broad emission band centered at 485 nm, and temperature induced electrical properties of the QD *4-(6-(diethylamino)-4-phenylquinolin-2-yl)benzoic acid* and TiO_2 films. The combination of QD with TiO_2, both layers in the form of thin film, forms a heterostructure in a very convenient format for integration in optoelectronics. Due to the techniques used for film deposition, both sort of films present defects, which are responsible for the electrical characteristics. The dominant level for TiO_2 is located about 760 meV from the conduction band bottom, inside the bandgap, whereas for the QD film the activation energy is about 328 meV. Both levels show up for a range above room temperature. In the first case, it suggests the second ionization level of oxygen vacancies (V_O^{2+}) or the third ionization level of interstitial titanium ions (Ti^{3+}), considering that both are electron donors, whereas in the case of QD it suggests a mechanism of small polaron tunneling (SPT).When combined as a heterostructure and explored under transport profile perpendicular to the films (transverse contacts) it leads to current-voltage (I-V) rectifying behavior similar to a *p-n* junction, which is evidence of the p-type-like electrical behavior of the QD, even though this I-V behavior may be destroyed for repetitive I-V measurement, which seems to be related with aging and the presence of defects at the heterostructure interface.

Keywords: *Titanium dioxide, Defects, Quinoline derivative, Heterostructure, Organic-inorganic.*

1. Introduction

Titanium dioxide (TiO_2) application reports have been published in several areas, ranging from photocatalysts for use in environmental issues and renewable energy production[1] to solar cells[2] among others[3]. The properties of this semiconductor oxide are directly related to its phases and possible amorphous and/or crystalline configurations. The main TiO_2 phases are anatase and rutile[4]. The rutile structure is thermodynamically more stable and with thermal annealing at higher temperatures or longer treatments, it becomes predominant in the samples, with the reorganization of anatase or brookite phases[5]. The bulk Gibbs free energy of the rutile phase is lower than that found for the anatase phase, but the surface energy of anatase is lower than that of rutile, which means that in the crystallization process the anatase phase initiates nucleation at lower temperatures. From some critical volume the formation of rutile crystals is favored to the growth of anatase crystals[6,7]. The anatase-rutile transition can be facilitated by reducing the pH of the precursor solution[8], so the interaction between the crystal surface and hydroxyl species inhibits anatase growth, favoring the more stable phase (rutile). Anatase has an indirect bandgap of about 3.25 eV whereas rutile has a direct bandgap of about 3.0 eV. Both phases have a tetragonal configuration[9,10]. The bands present in the photoluminescence (PL) spectra are strongly dependent on the thermal annealing temperature and crystalline phase, being about 550 nm, characteristic of anatase phase and 800 nm, related to the presence of rutile phase[10].

TiO_2 presents low electron mobility and rather more efficient transport in the anatase phase compared to rutile[11]. This is related to energy levels of trap states in rutile, which are very deep. Activation energies of 79 meV and 352 meV were obtained for anatase and rutile TiO_2, respectively[12]. Thin films exhibit thermally activated conduction in the region between 310 K and 468 K[13], where the sharp increase in the current comes from electrons released from oxygen vacancies and interstitial atoms of Ti^{3+}, both defects acting as donors in the TiO_2 matrix[12], even though the Ti^{3+} ion is a deeper level in the bandgap[14]. For lower temperatures, other transport mechanisms dominate, such as variable-range hopping (VRH) and tunneling[11,13,15], and the conductivity is not characterized by constant activation energy[13]. Excitation with distinct energy sources leads to distinct behaviors of the photo-induced current in heavily Yb-doped TiO_2[7], with regimes of domination of electron– hole pair generation or

*e-mail: scalvi@fc.unesp.br

intra-bandgap defects. Nanoparticles of TiO_2 may present different colors by controlling Ti^{3+} defects as well as defects correlated to oxygen vacancies (Vo), and the PL spectra in the region 500–580 nm depends strongly on the proportion of Ti^{3+}/Vo[16]. It has been reported that the bandgap of TiO_2 may be reduced by changing oxygen activity and the corresponding defect disorder[17], associated with strongly reducing environment during processing. This effect is related to structural relaxations around the defects, mainly oxygen vacancies and generation of larger defect aggregates. Titanium interstitials and oxygen vacancies form donor-type centers, while titanium vacancies exhibit acceptor-type properties. Below the conduction band minimum, DFT calculations rules[18] that the position of the defects inside the gap depends strongly on the Fermi level position and temperature. The first ionization level of Ti interstitial atoms is resonant with the conduction band whereas the second and third ionization levels have energies 0.52 eV and 0.78 eV, respectively, below the conduction band minimum. The oxygen vacancies have the first ionization level at 0.47 eV and the second level at 0.89 eV from the conduction band bottom[18].

Quinolinic derivatives (QD) in the form of thin film show promising characteristics due to good electrical conductivity, flexibility and high transparency[19,20], and have been efficiently applied in organic electronics and optoelectronics, where they may generate highly efficient electron transport materials due to their lower LUMO levels[21]. The quinolinic nucleus is present in a wide variety of natural products and drugs[22,23] and holds in its central structure an aromatic aza-heterocyclic with a benzene ring fused in positions 2 and 3 of a pyridinic ring. This structure leads quinoline derivatives to present electron acceptors and behave as p-type semiconductors[24]. Their luminescence in the blue range[25] is an attractive characteristic to photonics and light-emitting diodes[26]. The Stokes shift relative to the energy difference between emission and absorption bands is associated to the excited state decay to a lower energy state before emission[27]. As examples of p-type behavior of quinoline, it may be quoted 4H-pyrano[3,2-c][28] and Benzo[*de*] isoquino[1,8-*gh*] [29]. Structurally, QDs may have different compounds attached to main molecule, however they have characteristics in common: the presence of phenyl function, double bonds between carbon and oxygen and emission in the blue range.

Quinoline derivative have been used to bult heterojunction diodes with p-type Si. The threshold voltage is quite low when forward biased and strongly temperature dependent. The operating conduction mechanism is thermionic emission[28]. AC conductivity investigated as function of frequency (range 10^2–10^5 Hz) increases with increasing frequencies for all investigated ligands, for QD films deposited by spin coating. The correlated barrier hopping (CBH) is the dominant conduction mechanism for ligand 5-(2-(4-methoxyphenyl) diazenyl) quinolin-8-ol, 5-(2-(4-methylphenyl) diazenyl) quinolin-8-ol. and 5-(2-(4-chlorophenyl) diazenyl) quinolin-8-ol., while for ligands 5-(2-phenyldiazenyl)quinolin-8-ol and 5-(2-(4-nitrophenyl)diazenyl)quinolin-8-ol. the small polaron tunneling (SPT) mechanism dominates electrical transport[30].

In this paper, thin films of QD *4-(6-(diethylamino)-4-phenylquinolin-2-yl) benzoic acid* and the inorganic semiconductor oxide TiO_2, are electrically investigated individually or forming a heterostructure with characteristics behavior of *p-n* junction. Both films have strong temperature dependent electrical conduction with activation energies of 328 m eV and 760 meV for the QD film and the TiO_2 film respectively, and The QD has emission in the blue range.

2. Materials and Methods

2.1. Preparation of solutions of TiO_2 and quinoline derivative 4-(6-(diethylamino)-4-phenylquinolin-2-yl)benzoic acid

15 mL of isopropyl alcohol and 0.70 mL of 65% nitric acid, from Synth, were added to 48 mL of distilled water. This mixture was kept under magnetic stirring, and 4 mL of titanium isopropoxide (IV) (Sigma Aldrich) was added slowly, remaining stationery for 30 minutes. At this point, an extremely quick formation of white precipitates is observed. After that, the remaining solution is subjected to a temperature of 35 ºC and magnetically stirred until a bluish, translucent, and homogeneous solution is formed. Finally, 1 mL of Triton X-100 (Sigma-Aldrich) surfactant is added, to obtain a suspension with greater dispersion of the colloids. This surfactant led to films with greater homogeneity due to the increased adhesion of the films to the substrate[31]. The formation of micelles avoids agglomeration of particles and provides homogenization of the surface morphology in the film deposition.

The synthesis of the quinoline derivative *4-(6-(diethylamino)-4-phenylquinolin-2-yl)benzoic acid* was done following a published procedure[32], where in a Erlenmeyer flask, 5 mmol of the aniline *N,N-Diethyl-p-phenylenediamine* and the aldehyde *4-Formylbenzoic acid* are added, thus forming a Schiff base, followed by the addition of 5 mmol of *phenylacetylene* plus 1 mL a 0.5 M solution of *hydrochloric acid*. This solution is kept in agitation in a bath at 130ºC for 72 hours. The reaction between the Schiff base and *phenylacetylene* in an acidic medium has quinoline as its product. After this procedure, it is necessary to separate the quinoline obtained from the reactants and impurities. The chosen technique to carry that out was reactive extraction. First, a solution of saturated sodium bicarbonate and ethyl acetate are added to stop the reaction and then a solution of sodium hydroxide is added, because by increasing the alkalinity, the separation of phases, between aqueous and organic takes place. With the help of a separation funnel, the aqueous phase is collected, 10 mL of water is added to the organic phase until there is no longer a significant amount of product left. This aqueous phase is acidified with a 2M hydrochloric acid solution and becomes neutral once it was in alkaline medium. From this solution, the desired quinoline derivative is extracted by the addition of an organic solvent that makes a strong bond with the QD and a weak bond with water. In this case, 5 mL of ethyl acetate was added and the new formed phase (quinoline derivative plus solvent) was removed from the separation funnel. This last step was repeated 3 times. Then, the solvent is left evaporate, leaving the quinoline with a high degree of purity, which is recrystallized in methanol and filtered, leading the quinoline derivative in powder form with yellowish-

brownish color (52% yield). More details on the obtainment of the quinoline derivative can be found elsewhere[32] and the procedure to separate the QD from impurities can be seen in the supplementary material (Figure S1).

Previously to deposition in the form of thin films, the QD powder was solubilized in the organic solvents THF (tetrahydrofuran) and acetone with a concentration of 1 mg/mL, which present high solubility with quinoline and low boiling points. These solvents are chosen because acetone and THF are aprotic solvents, where hydrogen is bonded only to carbon, making them donors of electron pairs, which allows the solvation of a cation derivative[33], which in the case of the present work, is the quinolinic derivative. Other solvents such as isopropanol and ethanol have also been tested, but they are protic polar solvents, and the bonds between hydrogen and very electronegative elements, such as oxygen, fluorine and nitrogen, leave H^+ in solution. As a result, the solubilization is not complete and the surface covering with the deposited film is flawed and therefore they were not used in the present work.

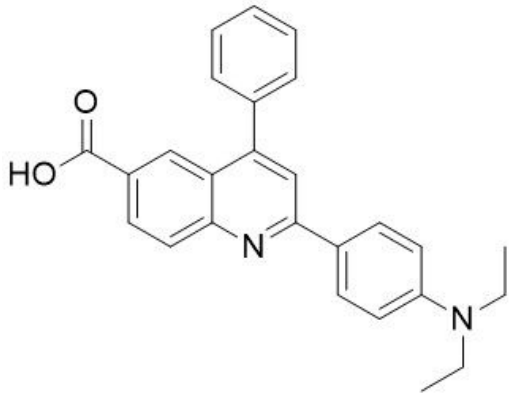

Figure 1. Quinoline derivative 4-(6-(diethylamine)-4-phenylquinolin-2-yl) benzoic acid.

2.2. Sample assembly

Deposition of both thin films of TiO_2 and quinoline derivative were performed on borosilicate glass substrates with a top of FTO (fluorine doped tin dioxide) layer by the dip-coating technique in the case of TiO_2 and spin-coating in the case of QD. For the TiO_2 film, it was used a MQB SG 1/302 pump, linked to a Microprocessor controller MQCTL2000-MP. The immersion rate was 10 cm/min and the number of layers is 3. After each layer the film is submitted to gelatinization process for 10 min and also to an intermediate thermal annealing at 110 °C for 10 min. After the deposition of the last layer a final annealing at 500 °C for 5 h is done in a EDGCOM 3P oven. The final thickness is about 400 nm.

For the quinoline derivative *4-(6-(diethylamine)-4-phenylquinolin-2-yl) benzoic acid,* solubilized in THF or acetone, deposition was performed on etched FTO and silica substrates. The spin-coating was performed in a Laurell Technologies Spin Coater equipment, in which 0.5 mL of the solution was deposited on top of the substrate, followed by rotation at a rate of 3000 rpm for 30 sec in an inert nitrogen atmosphere. After each layer, in a total of 5 layers, samples were heated for 5 min at a temperature of 70° C to evaporate the solvent. After the last layer, the annealing time is 20 min. The final thickness is about 200 nm. Figure 1 is the chemical formula of the quinoline derivative used in this work.

FTO is used due to its low electrical resistance (about 45 Ω/mm), allowing to be used as efficient electrical contacts. The central FTO region was removed, creating a channel that was later filled with TiO_2 or DQ, as seen in Figure 2(a). To protect the sides containing FTO from corrosion, Kapton polyamide tape was used, and metallic zinc was inserted in the unwanted region. Hydrochloric acid (HCl) was subsequently poured over this region. Zinc acts as a catalyst for the etching process that results in the total elimination of the FTO layer from the channel [34].

Thin films of TiO_2 and QD were also arranged in a heterostructure, as seen in Figure 2(b). The same layout of the bottom deposited layer was used, similar to samples for

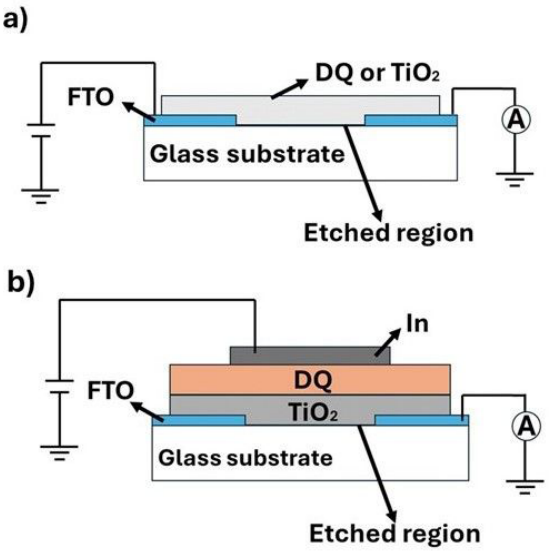

Figure 2. (a) Layout for the device assembly in the case of individual layers. (b) Layout for the heterostructure of TiO_2 and DQ thin films, deposited on glass with lower etched FTO contacts and top In contact.

individual investigation of films. One shall notice that only one bottom contact is used for electrical connections, which can be supposed as a quasi in plane conduction device. The number of layers as well as the thermal annealing time and temperature follow the procedure for individual layer of each of these compounds. The sample design aims verifying the electrical behavior of the device through the interface, in this case using evaporated Indium (In) as metallic contact on the superior surface of the quinoline derivative. It makes the electrical transport mandatory to occur in both materials and through the interface. Such a configuration allows verifying the rectifying characteristic of a *p-n* junction, since TiO_2 is naturally n-type and QD is expected to act as a p-type semiconductor.

2.3. Sample characterization

For optical absorption and excitation measurements of the solutions in the UV-Vis range, the Agilent Cary Eclipse

fluorescence spectrophotometer was used, which comprises a Xenon flash lamp for sample excitation.

Optical transmittance measurements on the films were performed using a Perkin Elmer spectrophometer, model Lambda 1050 Uv/Vis/Nir, in the range 200-1800 nm (scanning in the direction of increasing energy). With the transmittance data, the optical absorption coefficients were evaluated and the bandgap of TiO_2 and DQ film were calculated using the Tauc plot[35].

Current–voltage and current as function of temperature measurements were carried out in two configurations: 1) for the quinoline derivative films it was used a hotplate IKA model RH-KT/C and the temperature control was done using manually with Minipa multimeter model ET-207 under room atmosphere conditions; 2) for the TiO_2 film, it was used a closed Helium circuit cryostat from Janis Research, under room atmosphere conditions or with pressure of about 10^{-5} torr, coupled to a Lake Shore Cryotronics temperature controller with 0.5 °C of precision. In both cases, it was used Keithley electrometers models 6517 and 6517A for film biasing and collecting of electrical current.

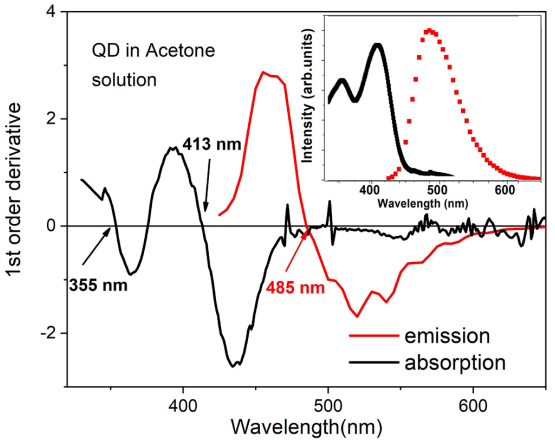

Figure 3. First derivative of optical absorption and emission spectra of quinoline derivatives solubilized in acetone. Excitation for the emission spectrum at 413 nm. Inset: optical absorption and emission.

3. Results and Discussion

Fluorescence measurements data of the QD in acetone solution are sown in Figure 3. Data are plotted in the format of 1st derivate which reveals effective rate of molecule excitation and recombination. Experimental data are displayed in the inset of Figure 3. There is no significative shift for solubilization in THF. The excitation energy for the emission spectra was kept at the highest absorption band of QD solubilized in acetone: 413 nm. A 72 nm Stokes shift is observed, and it is related to the relaxation of the excited level to a lower energy state[36]. The labeled points in Figure 3 are the band maxima, which means that the first derivative is zero. The emission is clearly in the blue region. For the absorption, the bands are generated by electron-hole pairs excitation, with highest rate in the UV region (about 400 nm), whereas the emission band is related to electron-hole recombination about 450 nm, still in the blue region. Absorptions in the ultraviolet range (355 nm in Figure 3) are attributed to transitions of molecular orbitals, particularly the conjugated double bonds present in the structure of quinoline derivative molecules[37].

Figure 4 shows transmittance curves of the films formed by five layers of QD deposited on silica, from the solubilization in acetone and THF, with 3000 rpm of rotation rates. The absorption bands are the local minima and are labeled in Figure 3. They are observed for wavelengths about 305 and 430 nm and are in good agreement with the absorption spectra in the solution (Figure 3), which assures that films are effectively deposited. The inset in Figure 4 is the Tauc Plot, by considering direct transition, where the squared optical absorption coefficient times the energy of the incident light, $(\alpha h\nu)^2$ is plotted as function of the energy of the incident light, yielding a bandgap energy of about 2.42 eV. For this evaluation it was considered the highest rate of electron-hole pairs generation (maximum first derivative), that takes place at the fundamental optical absorption edge, which means the most at right portion of the curve, since for the others linear parts, the excited transition rate decreases. A similar

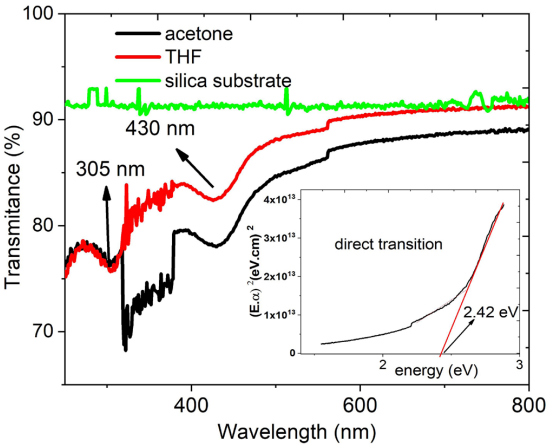

Figure 4. Transmittance curves of silica substrate, and QD films with five layers deposited by spin coating, from precursor solution of acetone and THF. **Inset:** Tauc plot with direct bandgap evaluation.

plot considering indirect transition yields a bandgap in the order of some tenths of eV, which does not seem realistic. The obtained bandgap value is in fair agreement with the literature. El-Ghamaz et al.[30], working near the absorption edge with azo quinoline derivatives obtained the optical energy gap in the range of 1.34–2.26 for direct transition, whereas EL-Shabaan and Gaml[38] investigating quinoline carboxylate derivative found the best fit for experimental data assuming indirect bandgap transition with the lowest value of the energy gap of. 3.36 eV. It is clear that the fundamental absorption edge and the sort of dominant transition is highly dependent on the type of organic ligand on the quinoline.

Figure 4 allows observing that films deposited with 5 layers present a pronounced drop in transmittance, mainly about 305 nm and 430 nm, independent on the used solvent, The absorption band at 430 nm refers to the fundamental absorption edge, promoting valence band-conduction band

transition, whereas the band at 305 nm refers to other electronic transitions between different states[37]. The 5 layers deposition ensures that the whole substrate has been effectively filled with deposited material and, then effective illumination takes place. The bandgap evaluation for TiO_2 film is shown in the supplementary material (Figure S2), where it is considered anatase structure and indirect bandgap, yielding about 3.35 eV.

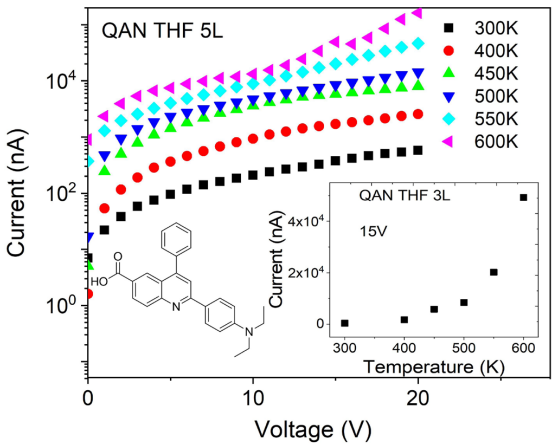

Figure 5. Electric current as function of voltage at several temperatures, for quinoline derivative sample (QAN) with 5 deposited layers by spin-coating. Left Inset: QD chemical formula Right inset: Current as function of temperature for a fixed bias.

Current as a function of applied voltage at different temperatures are shown in Figure 5 for QD with 5 deposited layers by spin-coating from THF solvent on FTO substrate. The left inset at Figure 5 is QD chemical formula and the right inset is the current as function of temperature at fixed bias of 15 V, evaluated from the curves of the main figure.

Figure 6(a) shows the current as function of temperature for a fixed bias of 10 V, for TiO_2 film and the inset is the Arrhenius Plot for this film, showing the activation energies for two temperature ranges. At the right side of Figure 6 there is a diagram showing the bandgap and the measured levels through the Arrhenius plot. Figure 6(b) is the Arrhenius plot for QD, obtained from the measured data shown in Figure 5. In Figure 5(a) the thermally activated conduction is evident in the region above room temperature, which is in good agreement with Yildiz et al.[13] that report thermally activated conduction between 310 K and 468 K for TiO_2, where the sharp increase in the current comes from electrons released from oxygen vacancies and interstitial atoms of Ti^{3+}, which are donors in the TiO_2 matrix[12]. For lower temperatures, other transport mechanisms dominate, such as variable-range hopping (VRH) and tunneling[11,13]. The obtained activation energy of 11.4 meV for lower temperature range may associated with these processes.

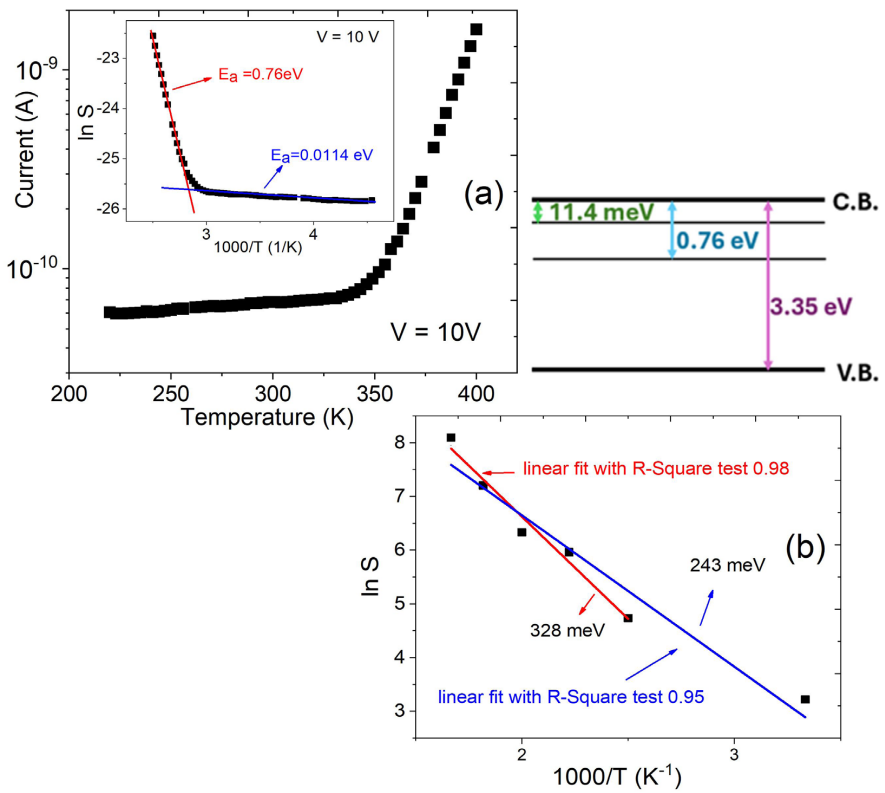

Figure 6. (a) Current as function of temperature for a fixed bias of 10 V, for TiO_2 film. Inset: Arrhenius Plot for this film, (right) Diagram showing the bandgap and the measured levels through the Arrhenius plot. (b) Arrhenius plot for QD.

The calculated activation energy for the TiO_2 film is about 0.76 eV below the conduction band bottom. This is in fair agreement with the third ionization level of Ti interstitial ion or the second ionization level of vacancies (0.78 eV and 0.89 eV from the conduction band bottom, respectively[18]). It is interesting to mention that X-ray diffractogram (not shown) displays the broad diffuse profile characteristic of nanocrystalline domain of grains, and the evaluated crystallite size is about 20 nm for deposition in borosilicate glass and thermal annealing at 500 °C, and 50 nm for deposition on silica substate and thermal annealing at 1000 °C, both evaluated in the plane (101) of the anatase phase, which is the most intense. Then, such small crystallites lead to a quite intense grain boundary scattering that decreases the mobility. The combination of defects must be taken into consideration concomitant with small crystallites since the defect levels may be affected by the ion location and its neighborhood. It may be an explanation by the change in the inclination of the Arrhenius curve as the temperature gets lower, which means a close distribution of defect levels.

In the case of QD film the activation energy in the region of higher temperature, 400 to 600 K, yields activation energy of 328 meV, with T-square test of 0.98. This is in excellent agreement with El Ghamaz et al.[30] report which gives an activation energy of 330 meV for samples dominated by small polaron tunneling (SPT) model. As the temperature of 300 K (1000/T = 3.33 K^{-1}) is included in the linear fit, the activation energy decreases to 243 meV and the R-square test gets worse (0.95). This is also consistent with the analysis by El Ghamaz et al, that found two levels, associated with two temperature ranges, and the lower temperature level presents lower activation energy. The decrease of the activation energy in Figure 6(b), and the decrease in the linearity leads to interpret as the existence of two levels in the QD, which means that 300 K is about an intermediate temperature between them. The more defined thermal excitation only above room temperature may be related to the promotion of electrons from HOMO (highest occupied molecular Orbital – valence band) to LUMO (lowest unoccupied molecular orbital - conduction band). Considering the type of deposition used here, this bandgap may be affected the Urbach energy, which may be high, and it is related to the structural quality of a material. In photovoltaic devices, the correlations between the static disorder given by the Urbach tail and the device performance are related to an appropriate molecular design[39]. In the present case the optimization of the compounds attached to main molecule may improve the performance of *p-n* junctions for optoelectronic applications.

Figure 7(top) shows transverse electrical characterization according to the device setup shown in Figure 2. Figure 7(bottom) is the energy band diagram at TiO_2/QD interface, where the interface potential barrier, responsible for the I-V curve behavior as observed. This diagram represents the thermodynamical equilibrium condition (previously to external applied bias) with the Fermi level equality along the device. Concerning the Figure 7(top), in the first series of data, a rectifying behavior is observed for negative bias (full black circles), and a there is a tendency to current conduction for forward bias, even though, the diode behavior is not clear yet. In the second data colleting (full red circles in Figure 7(top)) the

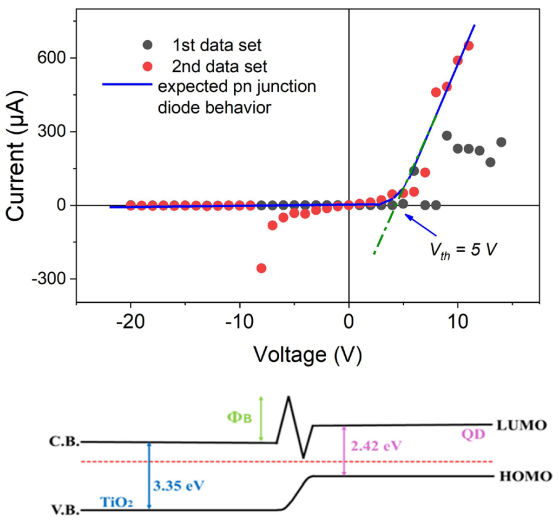

Figure 7. (top) current voltage for the heterostructure TiO2/QD. (bottom) simplified energy band diagram, showing the measured bandgaps and the interface potential barrier (Φ_B).

diode behavior is more evident for positive bias, when the positive pole is in the quinoline derivative layer, with a threshold voltage of about 5 V. When the sample is negatively polarized, the rectifying behavior is repeated, however about 8 V a reverse breakdown seems to take place. Although for most diodes the breakdown is not a detrimental effect, as far as the polarization does not last for a long time[40], in the case of the TiO_2/QD diode it seems that the junction is destroyed for some voltage magnitude, what justify the quite low current observed for bias lower than -8 V. This is consistent with a third measurement (Figure S3 in the supplementary material file) that shows an ohmic behavior for this device, destroying the diode-like behavior. Moreover, the magnitude of the current in the third data collecting is nanoA whereas for the forward bias in Figure 7 it is in the order of microA. Then, although the results reported in Figure 7 are in good agreement with the p-type behavior of the quinoline derivative, and points consistently to the possibility of building an organic-inorganic *p-n* junction, the aging caused by Joule effect seems to be affecting the QD layer, and the ways to avoiding such a negative effect is under investigation.

There are plenty of defects in both sort of materials and consequently the interface between the layers is possibly covered with dangling bonds. Under excitation with bias higher than the threshold voltage or photo-induced, these bonds may recombine and destroy the interface barrier, yielding electrical conduction between layers with no barrier. However, due to the large concentration of defects all over the materials the conductivity is low, related to high carrier scattering phenomena. This is unlike the forward bias through the interface barrier with injects electrons from the n-side to p-side and in opposite direction for holes, giving rise to the much higher current, as observed in the first measurements.

It is interesting to mention at this point that nanosized titanium dioxide prepared by sol-gel method has been used for photocatalytic degradation of quinoline[41], which has been

improved when titanium dioxide/graphene oxide composites are used concomitant with visible light irradiation[42]. It may be the cause of the vanishing of the rectifying behavior seen in Figure 7, what must be carefully investigated since it depends on the used ligand. In this case, for efficient use of this sort of heterostructure for optoelectronic application, an intermediate layer can be proposed, that avoids the direct contact between QD and TiO_2 film, which is matter for future research.

4. Conclusion

Absorption bands of the quinolinic derivative (QD) *4-(6-(diethylamine)-4-phenylquinolin-2-yl) benzoic acid* are in UV region whereas the emission of this compound occurs in the blue range, which can be explored in LEDs.

Both sort of films presents a high defects density, and the dominant level for TiO_2 is about 760 meV from the conduction band bottom, inside in the bandgap. It corresponds to the second ionization level of oxygen vacancies (V_O^{2+}) or the third ionization level of interstitial titanium ions (Ti^{3+}), considering that both are electron donors in the TiO_2 matrix. In the case of QD film, the activation energy is about 328 meV, a value in very good agreement with a mechanism of small polaron tunneling (SPT).

The electrical behavior of the combination of SnO_2 with this type of QD forming a heterostructure leads to a rectifying behavior similar to a *p-n* junction, when explored under transport profile perpendicular to the films (transverse contacts). It is also evidence of the p-type-like electrical behavior of the QD, and this combination of materials and has shown high applicability in several types of possibilities such as blue LED or transparent *p-n* junction.

Although the rectifying characteristics may be destroyed for repetitive application of IxV measurement, which seems to be related with the presence of defects at the heterostructure interface, these results show the potentiality of this combination.

5. Acknowledgements

Authors acknowledge Prof. Luiz C. Silva Filho and Lucas M. Martins for fruitful discussions, and Dr. Vitor Fernandes Moreno for the help with quinoline samples preparation. Authors acknowledge also CNPq (proc. 303388/2022-6) and FAPESP (proc. 2022/08483-0 and 2022/12998-5) for financial support (scholarships).

6. References

1. Dincer I, Acar C. Innovation in hydrogen production. Int J Hydrogen Energy. 2017;42(22):14843-64.
2. Kharel PL, Zamborini FP, Alphenaar BW. Enhancing the photovoltaic performance of dye-sensitized solar cells with rare-earth metal oxide nanoparticles. J Electrochem Soc. 2018;165(3):H52-6.
3. Haider AJ, Jameel ZN, Al-Hussaini IH. Review on: titanium dioxide applications. Energy Procedia. 2019;157:17-29.
4. Dewhurst JK, Lowther JE. High-pressure structural phases of titanium dioxide. Phys Rev B. 1996;54(6):3673.
5. Bakri A, Sahdan AMZ, Adriyanto F, Raship NA, Said NDM, Abdullah SAM, et al. Effect of annealing temperature of titanium dioxide thin films on structural and electrical properties. AIP Conf Proc. 2017;1788(1):030030.
6. Ding K, Miao Z, Hu B, An G, Sun Z, Han BZ. Study on the anatase to rutile phase transformation and controlled synthesis of rutile nanocrystals with the assistance of ionic liquid. Langmuir. 2010;26(12):10294-302.
7. Pedrini LFK, Santos SBO, Trino LD, Scalvi LVA. Anatase–rutile transition and photo-induced conductivity of highly yb-doped tio$_2$ films deposited by acid sol–gel dip-coating method. J Electron Mater. 2020;49(11):6360-79.
8. Yudoyono G, Zharvan V, Ichzan N, Daniyati R, Indarto B, Pramono YH, et al. Darminto, Influence of pH on the formulation of TiO_2 powder prepared by co-precipitation of $TiCl_3$ and photocatalytic activity. AIP Conf Proc. 2016;1710(1):030011.
9. Wu YN, Jeffrey K, Wuenschell JK, Fryer R, Saidi WA, Ohodnicki P, et al. Theoretical and experimental study of temperature effect on electronic and optical properties of TiO_2: comparing rutile and anatase. J Phys Condens Matter. 2020;32(40):405705.
10. Ramos RA Jr, Boratto MH, Li MS, Scalvi LVA. Emission properties related to distinct phases of sol-gel dip-coating titanium dioxide, and carrier photo-excitation in different energy ranges. Mater Res. 2017;20(4):866-73.
11. Mardare D, Baban C, Gavrila R, Modreanu M, Rusu G. On the structure, morphology and electrical conductivities of titanium oxide thin films. Surf Sci. 2002;507:468-72.
12. Wang X, Feng Z, Shi J, Jia G, Shen S, Zhou J, et al. Trap states and carrier dynamics of TiO_2 studied by photoluminescence spectroscopy under weak excitation condition. Phys Chem Chem Phys. 2010;12:7083-90.
13. Yildiz A, Lisesivdin S, Kasap M, Mardare D. Electrical properties of TiO2 thin films. J Non-Cryst Solids. 2008;354:4944-7.
14. Bharti B, Kumar S, Lee HN, Kumar R. Formation of oxygen vacancies and Ti^{3+} state in TiO_2 thin film and enhanced optical properties by air plasma treatment. Sci Rep. 2016;6:32355.
15. Bak T, Nowotny MK, Sheppard LR, Nowotny J. Mobility of electronic charge carriers in titanium dioxide. J Phys Chem C. 2008;112:12981-7.
16. Dwivedi C, Mohammad T, Kumar V, Dutta V. Ti^{3+} and oxygen defects controlled colored TiO_2 nanoparticles by continuous spray pyrolysis. Vacuum. 2020;182:109612.
17. Nowotny J, Alim MA, Bak T, Idris MA, Ionescu M, Prince K, et al. W. Sigmund W, Defect chemistry and defect engineering of TiO2-based semiconductors for solar energy Conversion. Chem Soc Rev. 2015;44:8424.
18. He J, Behera RK, Finnis MK, Li X, Dickey EC, Phillpot S Sr. B. Sinnott SB, Prediction of high-temperature point defect formation in TiO2 from combined ab initio and thermodynamic calculations. Acta Mater. 2007;55:4325-37.
19. Mahmoud A, Darwish A, Qashou SJ. Film thickness effects on nanorods organic films of azo quinoline derivatives for optical applications. Prog Nat Sci. 2019;29(4):402-9.
20. Zeyada HM, El-Taweel FM, El-Nahass MM, El-Shabaan MM. Effect of substitution group on dielectric properties of 4H-pyrano [3, 2-c] quinoline derivatives thin films. Chin Phys B. 2016;25(7):077701.
21. Dumouchel S, Mongin F, Trécourt F, Quéguiner G. Tributylmagnesium ate complex-mediated bromine–magnesium exchange of bromoquinolines: a convenient access to functionalized quinolines. Tetrahedron Lett. 2003;44:2033-5.
22. Michael JP. Quinoline, quinazoline and acridone alkaloids. Nat Prod Rep. 2007;24:23-246.
23. Pandeya SN, Tyagi A. Synthetic approaches for quinoline and isoquinoline. Int J Pharm Pharm Sci. 2011;3(3):53-61.
24. Lewinska G, Sanetra J, Marszalek KW. Application of quinoline derivatives in third-generation photovoltaics. J Mater Sci Mater Electron. 2021;32:18451-65.
25. Raut SB, Dhoble SJ, Park K. Amino diphenyl quinoline: a promising blue emitting organic luminescent material. Indian J Phys. 2013;87:19-23.

26. Koścień E, Sanetra J, Gondek E, Jarosz B, Kityk IV, Ebothe J, et al. Optical poling of several halogen derivatives of pyrazoloquinoline. Opt Commun. 2004;242(4-6):401-9.
27. Alarcon RT, Santos GC, Oliveira AR, Silva-Filho LC, Bannach G. Synthesis of luminescent polymers in the UV light region from dimethacrylate monomer using novel quinoline dyes. J Appl Polym Sci. 2019;136:47461.
28. Zeyada HM, El-Nahass MM, El-Shabaan MM. Photovoltaic properties of the 4H-pyrano[3,2-c]quinoline derivatives and their applications in organic–inorganic photodiode fabrication. Synth Met. 2016;220:102-13.
29. Baranov DS, Popov AG, Uvarov MN, Kulik LV. Synthesis of benzo [de] isoquino [1, 8-gh] quinolines and light-induced electron transfer in their composites with conductive polymer poly (3-hexylthiophene). Mendeleev Commun. 2014;24(6):383-5.
30. El-Ghamaz NA, El-Bindary AA, El-Sonbati AZ, Beshry NM. Geometrical structures, thermal, optical and electrical properties of azo quinoline derivatives. J Mol Liq. 2015;211:628-39.
31. Fonseca LP, Pedrini LFK, Lima JVM, Escaliante LC, Santos SBO, Scalvi LVA. Enhancement of surface properties of sol gel tin dioxide thin films with addition of surfactant in the precursor solution. Appl Phys, A Mater Sci Process. 2021;127:503-12.
32. Martins LM, Moreno VF, Rosário IS, Graeff CFO, Silva Filho LC. Bronsted acid mediated facile greener multicomponent synthesis of 2,4-diaryl-quinoline derivatives in water, orbital: electron. J Chem. 2021;14(1):1-9.
33. Rossini E, Knapp E-W. Proton solvation in protic and aprotic solvents. J Comput Chem. 2016;37:1082-91.
34. Kotok VA, Malyshev VV, Solovov VA, Kovalenko VL. Soft electrochemical etching of FTO-coated glass for use in Ni (OH) 2-based electrochromic devices. ECS J Solid State Sci Technol. 2017;6(12):772.
35. Tauc J. Optical properties and electronic structure of amorphous Ge and Si. Mater Res Bull. 1968;3:37-46.
36. Czaplinska C, Maron A, Malecki JG, Szafraniec-Gorol G, Matussek M, Malarz K, et al. Comprehensive exploration of the optical and biological properties of new quinoline based cellular probes. Dyes Pigments. 2017;144:119-32.
37. Liang F, Chen J, Cheng Y, Wang L, Ma D, Jing X, et al. Synthesis, characterization, photoluminescent and electroluminescent properties of new conjugated 2,2′-(arylenedivinylene)bis-8-substituted quinolines. J Mater Chem. 2003;13:1392-9.
38. El-Shabaan MM, Gaml EA. Fluorescent quinoline carboxylate derivative: study on the optical properties and photo diode application. Physica B. 2022;626:413578.
39. Zhang C, Mahadevan S, Yuan J, Ka J, Ho W, Gao Y, et al. Unraveling urbach tail effects in high- performance organic photovoltaics: Dynamic vs Static Disorder. ACS Energy Lett. 2022;7:1971-9.
40. Sze SM. Semiconductor devices physics and technology. New York: Wiley & Sons; 1985
41. Jing J, Feng J, Li W. Kinetic study of photocatalytic degradation of quinoline over nanosized titanium dioxide. J Fuel Chem Technol. 2012;40:380-4.
42. Jing J, Zhang Y, Li W, Yu WW. Visible light driven photodegradation of quinoline over TiO2/graphene oxide nanocomposites. J Catal. 2014;316:174-81.

Supplementary material

The following online material is available for this article:

Supplementary Information - Procedure for to separate the quinoline derivative (QD) from impurities.